

Effect of distribution shape on the melting transition, local ordering, and dynamics in a model size-polydisperse two-dimensional fluid

Jackson Pame and Lenin S. Shagolsem

Citation: Chin. Phys. B, 2024, 33 (**7**): 074702. DOI: 10.1088/1674-1056/ad39c9
Journal homepage: http://cpb.iphy.ac.cn; http://iopscience.iop.org/cpb

What follows is a list of articles you may be interested in

On the spreading behavior of a droplet on a circular cylinder using the lattice Boltzmann method

Fan Yang(杨帆), Hu Jin(金虎), and Mengyao Dai(戴梦瑶)
Chin. Phys. B, 2024, 33 (**6**): 064702. DOI: 10.1088/1674-1056/ad3b7f

Dynamic modeling of cavitation bubble clusters: Effects of evaporation, condensation, and bubble—bubble interaction

Long Xu(许龙), Xin-Rui Yao(姚昕锐), and Yang Shen(沈阳)
Chin. Phys. B, 2024, 33 (**4**): 044702. DOI: 10.1088/1674-1056/ad181f

Molecular dynamics simulation of the flow mechanism of shear-thinning fluids in a microchannel

Gang Yang(杨刚), Ting Zheng(郑庭), Qihao Cheng(程启昊), and Huichen Zhang(张会臣)
Chin. Phys. B, 2024, 33 (**4**): 044701. DOI: 10.1088/1674-1056/ad08a7

Ferrofluid nucleus phase transitions in an external uniform magnetic field

B. M. Tanygin, S. I. Shulyma, V. F. Kovalenko, M. V. Petrychuk
Chin. Phys. B, 2015, 24 (**10**): 104702. DOI: 10.1088/1674-1056/24/10/104702

Electro–magnetic control of shear flow over a cylinder for drag reduction and lift enhancement

Zhang Hui (张辉), Fan Bao-Chun (范宝春), Chen Zhi-Hua (陈志华), Chen Shuai (陈帅), Li Hong-Zhi (李鸿志)
Chin. Phys. B, 2013, 22 (**10**): 104701. DOI: 10.1088/1674-1056/22/10/104701

Effect of distribution shape on the melting transition, local ordering, and dynamics in a model size-polydisperse two-dimensional fluid

Jackson Pame and Lenin S. Shagolsem[†]

Department of Physics, National Institute of Technology Manipur, Imphal, India

(Received 25 January 2024; revised manuscript received 24 March 2024; accepted manuscript online 3 April 2024)

We study the effect of particle size polydispersity (δ) on the melting transition (T^*), local ordering, solid–liquid coexistence phase and dynamics of two-dimensional Lennard–Jones fluids up to moderate polydispersity by means of computer simulations. The particle sizes are drawn at random from the Gaussian (G) and uniform (U) distribution functions. For these systems, we further consider two different kinds of particles, viz., particles having the same mass irrespective of size, and in the other case the mass of the particle scales with its size. It is observed that with increasing polydispersity, the value of T^* initially increases due to improved packing efficiency (ϕ) followed by a decrease and terminates at $\delta \approx 8\%$ (U-system) and 14% (G-system) with no significant difference for both mass types. The interesting observation is that the particular value at which ϕ drops suddenly coincides with the peak of the heat capacity (C_P) curve, indicating a transition. The quantification of local particle ordering through the hexatic order parameter (Q_6), Voronoi construction and pair correlation function reveals that the ordering decreases with increasing δ and T. Furthermore, the solid–liquid coexistence region for the G-system is shown to be comparatively wider in the T–δ plane phase diagram than that for the U system. Finally, the study of dynamics reveals that polydisperse systems relax faster compared to monodisperse systems; however, no significant qualitative differences, depending on the distribution type and mass polydispersity, are observed.

Keywords: polydispersity, ordering, phase diagram, dynamics

PACS: 47.57.–s, 87.10.Tf, 83.10.Rs, 87.15.Zg **DOI:** 10.1088/1674-1056/ad39c9

1. Introduction

Systems with varying particle shapes, sizes, masses, and other energetic properties are ubiquitous in nature. For instance, a complex heterogeneous environment as observed in cell membranes or cytoplasm consists of different constituents varying in shape/size and energetic parameters, and in colloidal systems in general. A simplified and generic coarse-grained fluid model serves as a convenient tool to study such complex systems, e.g., the Lennard–Jones (LJ) fluid model is able to explain the properties of argon, neon, binary mixtures, etc.[1–6] However, theory governing the melting and freezing transitions in a two-dimensional (2D) system has not yet been clearly understood.[7,8] In addition, whether the phase transition is of first or second order in nature is still debatable because the transition is interrupted by the formation of the hexatic phase.[9–14]

In polydisperse systems, added complexities in the system, e.g., formation of multiphase structures,[15] and slow relaxation[16] to overcome crystallization, also pose interesting challenges. Polydisperse LJ fluids exhibit a shift in transition parameters, such as solid–liquid transition temperature, with the formation of rich solid–fluid coexisting regions in the phase diagram along with enhanced fractionation and formation of new phases at larger cutoff.[15–18] The ordering and dynamics of such systems greatly rely on the nature of the interactions.[19,20] To comprehend this complex behavior, understanding the connection between the microscopic dynamics and the bulk properties is of utmost importance. On approaching the transition region, the motion of the particles drastically slows down, leading to structural arrest, which is reflected in the sudden increase in viscosity, as seen in glass formers.[21,22] Although ideal mode coupling theory has shed some light on microscopic dynamics, it still predicts the structural arrest at a certain critical value of temperature above the speculated glass transition temperature T_g.[23,24]

It is observed that the fundamental properties of almost all fluids are alike and rely not only on interactions but mainly on the local ordering[24,25] because spatial ordering is greatly influenced when particle size disparity is considered and changes with varying polydispersity. On the other hand, polydisperse systems with size distribution in the physical world often possess mass distribution. Theoretical studies of multi-component systems that address size-polydispersity such as colloids use a coarse-grained description to study the thermodynamic properties, such as free energy and phase diagrams.[26–30] Colloidal research has revealed a variety of novel colloidal crystalline and disordered states that can be achieved with square and triangular 2D substrates. The appearance of colloidal molecular crystal states in the substrate is presented in Refs. [31,32]. Colloidal studies have also shown to exhibit various ordered and partially ordered states such as star and pinwheel states which can be observed directly in experiments and can be adjusted by varying substrate strength. In ordered states, multistep melting occurs, with one species ro-

[†]Corresponding author. E-mail: slenin2001@gmail.com

© 2024 Chinese Physical Society and IOP Publishing Ltd

tating while the other remains orientationally ordered. Bose–Einstein condensates interacting with periodic substrates or superconductors with periodic pinning can likewise exhibit this phenomenon.[32] In another study, a particle-based model was used to study the dynamics of a sphere dimer, revealing its self-diffusiophoresis mechanism. The asymmetric distribution of catalytic activity led to an asymmetric gradient field, resulting in translational and rotational motion. The model revealed that systems with many dimers formed assemblies, with the chirality of the dimers playing a significant role in the formation of self assemblies.[33] In 2D, even size monodisperse LJ-fluid shows heterogeneous structure, heterogeneous dynamics, and complex behavior when close to its phase transition. The nature of phase transitions in 2D is still a point of contention when polydispersity is taken into account.[26,27,34]

While the majority of size polydisperse systems in nature follow log-normal distribution, a sizable fraction of them also follows Gaussian distribution. Size distributions of nanoparticles synthesized using chemical and physical routes are very close to Gaussian in nature.[35–38] Some examples include iron oxide nanoparticles[35] measured by dynamic light scattering and silver nanoparticles[36–38] determined from a TEM image. Uniform size distribution, on the other hand, can be considered as the extreme case where multiple Gaussian size distributed systems of similar peak height and very close means are distributed within a pair of upper and lower values. While log-normal distributions are cumbersome to work with analytically, Gaussian and uniform distributions are comparatively easier, and the lower and upper bounds to the particle size can be easily controlled latter. Thus, in this study, we focus our attention on the Gaussian and uniform size distributions of particles and study both static and dynamic properties of the system upon variation of polydispersity. In particular, we investigate the behavior of melting transition, growth/decay of crystallization with the variation in polydispersity through $\langle Q_6 \rangle$ and Voronoi construction. Recent studies on theory and numerical simulations indicate a temperature independent terminal polydispersity δ_t beyond which crystallization tends to vanish.[42,43] A lot of research has focused on polydispersity in size and their dynamics, which tend to alter the current understanding of the statics and dynamics of the pure systems by shifting the phase transition parameter and the nature of phase diagram. This is because polydispersity shifts the transition temperature towards higher values.[44] The present study aims to illuminate the various static and dynamic properties around the terminal polydispersity and the role of polydispersity in understanding the nature of coexistence phase diagram as observed through hexatic phase.

The remainder of the paper is organized as follows. In Section 2, we discuss the details of the simulation set-up and the model systems, and in Section 3, we discuss results on the behavior of thermodynamic transition temperature. Followed by discussion of spatial ordering, positional correlation and particle dynamics in Sections 4–6, respectively, and we finally conclude the paper in Section 7.

2. Model and simulation details

Constant NPT molecular dynamic (MD) simulations[45,46] are performed considering $N = 2500$–10000 number of coarse-grained particles. All the pair-wise interactions in the system are modeled via a LJ potential, defined as

$$U_{\rm LJ}(r) = 4\varepsilon \left[(\sigma_{ij}/r_{ij})^{12} - (\sigma_{ij}/r_{ij})^{6} \right] , \tag{1}$$

with r_{ij} the separation between a pair of particles i and j, ε (= 1, for all particles under consideration) is the depth of the potential, and $\sigma_{ij} = (\sigma_i + \sigma_j)/2$ is the effective diameter, where $\sigma_{i/j}$ is the diameter of particle i/j. The LJ potential is truncated and shifted to zero at a cut-off distance $r_c = 2.5\sigma_{ij}$. All the physical quantities used in this study are expressed in reduced units, where length is measured in units of $\langle\sigma\rangle$ (mean size), temperature T in units of ε/k_B with k_B Boltzmann constant, pressure in units of $\varepsilon/\langle\sigma\rangle^3$, and time in $\tau_{\rm LJ} = \sqrt{m\langle\sigma\rangle^2/\varepsilon}$ units.[45,46] Thus, by having the experimental values of interaction strength, size, and mass one can easily relate LJ reduced units to the corresponding real units.[46] In order to generate a size polydispersed system, we draw at random the value of particle diameter σ from a given distribution. In this study, we consider two types of distribution, namely,
(a) uniform distribution (U) defined as

$$P(\sigma) = \begin{cases} 1/(b-a), & \text{for } a < \sigma < b, \\ 0, & \text{otherwise}, \end{cases} \tag{2}$$

with mean $(a+b)/2$ and variance $(b-a)^2/12$, and
(b) Gaussian distribution (G) defined as

$$P(\sigma) = \frac{1}{d\sqrt{2\pi}} \exp\left[-\frac{1}{2} \left(\frac{\sigma - \langle\sigma\rangle}{d} \right)^2 \right], \tag{3}$$

with $d = \sqrt{\sigma - \langle\sigma\rangle}$ as standard deviation (SD) and $\langle\sigma\rangle$ as mean. In this study, we fix the mean particle size at 2.0 for both U and G systems and study the effect of varying the extent of size-polydispersity in the respective systems through the systematic variation of variance about the mean. Here, the degree of polydispersity is characterized by the polydispersity index (PDI), defined as the ratio of the SD to mean, i.e. $\delta = {\rm SD}/{\rm mean}$, which for U system reads $\delta = \frac{1}{\sqrt{3}}\left(\frac{b-a}{a+b}\right)$. In addition to size distribution, we also consider two cases of particle mass: (i) the same mass system, i.e., irrespective of sizes all particles have same mass of $m = 1$, and (ii) poly-mass, i.e., mass scales with size, e.g., mass of the $i^{\rm th}$ particle $m_i = (\pi\sigma_i^2/4)\rho_p$ with ρ_p the particle density which, for simplicity, we assume it to be unity. Since we study a $2d$ system, the value of projected area of a particle is assigned as its mass instead of the actual volume. A summary of the systems studied is presented in Table 1.

Table 1. System summary.

No. of particles N	2500–10000
Size distribution	(a) uniform
(mean value = 2)	(b) Gaussian
Particle mass m_i	(a) same mass ($m = 1$ for all)
	(b) poly-mass (scales with size)

For the above systems, constant NPT simulations are performed using Nosé–Hoover thermostat and barostat to maintain constant temperature and pressure, respectively. The pressure along X- and Y-directions is set to $P = 1.5$. The damping factors for thermostat and barostat are kept at 1.0 and 10.0, respectively. To update the position and velocity of the particles, we integrate the equations of motion using a velocity-Verlet scheme with an integration time-step of $\delta t = 0.005$. Initially, the systems at a given temperature are prepared at very low density and then slowly compressed to reach the target pressure. After reaching the desired P value, the systems are relaxed further for about 10^7 MD. The well equilibrated samples are then switched to constant NVT ensemble and perform production runs, which typically last for 10^7 MD steps or more. Switching to constant NVT ensemble is for convenience while calculating dynamical quantities such as mean-square displacement. All the simulations reported here are performed using the LAMMPS open-source code.[47] As a reference system, one-component (1C) system, i.e., size mono-disperse, is prepared following the same protocol described above. For the 1C system, we set the particle size and interaction energy to unity.

3. Thermodynamics

Simulation snapshots of typical equilibrated samples are shown in Fig. 1 at different values of δ for both G and U systems for T below the respective transition temperatures. Particles of similar sizes tend to group together forming mosaic-like structure as the polydispersity increases. Since we are interested in how the distribution in size and mass scaling affect the transition, we perform continuous heating-cooling cycles from $T = 0.1$ to 3.0 (under NPT condition) to locate the melting transition for all of the systems. The data reported here are for a system with $N = 5000$ particles (otherwise stated clearly), which is sufficiently large in the sense that no significant change in T^* is seen around this N value. The dependence of transition temperature on the system size is shown in supplementary Fig. S1.

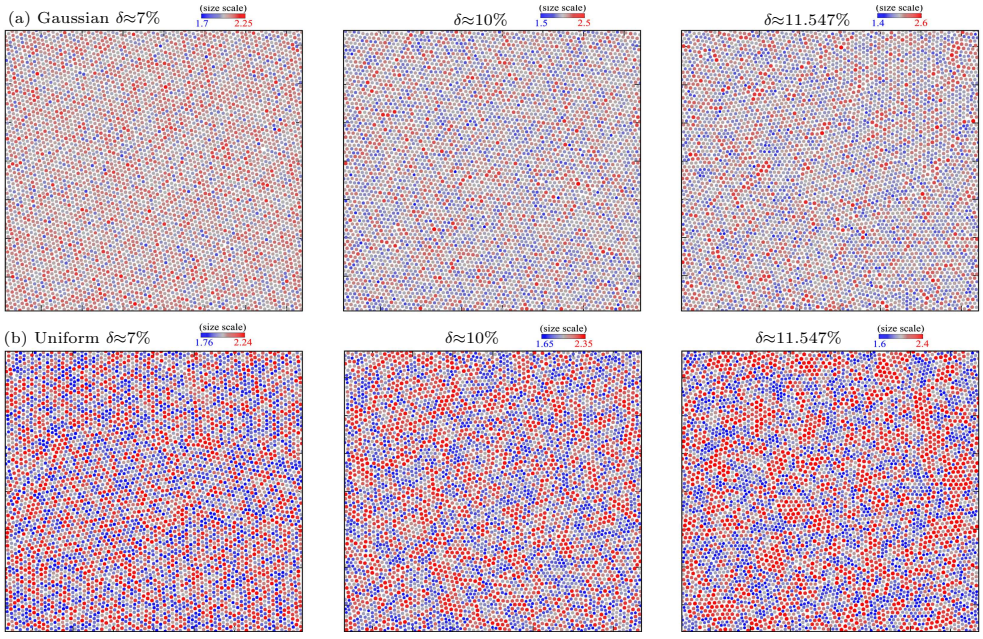


Fig. 1. Typical simulation snapshots of relaxed samples (a) Gaussian and (b) uniform systems at different δ values indicated in the figure, and $T = 0.4$ ($< T^*$) and number of particles $N = 5000$. Color bar indicates particle size distribution.

In Fig. 2, we display the plot of enthalpy H $(= u + Pdv)$ and heat capacity $C_P = (\partial H/\partial T)_P$ for systems. Here, u is the internal energy and v is the volume per particle. The maxima position of C_P curves gives the approximate value of thermodynamic transition temperature, T^*. As one can see, the introduction of mass polydispersity shows no significant effect in the value of T^* (except for height of C_P curve). For the pure 1C reference system we see $T^* \approx 0.57$ at $P = 1.5$ which is consistent with earlier study.[5] The transition temperature (T^*) increases as δ increases until $\delta \approx 2\%$ and then gradually decreases. This effect has also been seen in studies of model ionic liquids in which particle size polydispersity varies in the anion.[48] This is because with small introduction of δ, the packing efficiency is greatly enhanced, as shown in Fig. 3 ($\phi \approx 68.35\%$ for 1C and $\approx 74\%$ for G and U systems for $\delta \approx 0.5\%$ at $T = 0.5$). The sudden drop in the ϕ value corresponds to the temperature of the C_P peak for both the polydisperse systems where a solid melts to an isotropic liquid. On

further increasing δ, T^* diminishes rapidly due to decreasing particle correlation and the solid–liquid transition temperature drops gradually as it approaches the terminal polydispersity, as shown by the shift in the discontinuity of ϕ. This transition is also reflected by the heat capacity plot indicated by the sudden change in the enthalpy curve. The introduction of mass polydispersity shows no significant shift in the T^* value for the polydisperse systems (although differences appear in the intensity of C_P values but not the peak position) are observed, see Fig. 2(a). For the polydisperse systems, there is no significant difference in the ϕ value above their respective T^*, this is because the system is dominated by liquid phase for all δ at $T > T^*$.

For the G system, no significant difference in the C_P peaks for both the same mass and polydisperse mass systems is observed, see Fig. 2(a). In contrast, the C_P values for the U systems are relatively higher in magnitude when polydispersity in mass is introduced in the systems with no distinct shift in T^*. This indicates that the polydisperse mass systems require greater heat to undergo a phase change as compared to the corresponding mono-disperse mass systems. The differences in the C_P peak gradually decrease with increasing polydispersity (see Figs. 2(iii) and 2(iv)) for both the systems. The plot of T^* as a function of δ is shown in Fig. 4. It is observed that with increasing δ the value of T^* increases and remains roughly constant in a narrow interval 1%–2%, beyond which it gradually decreases and terminates at $\delta_t \approx 8\%$ (U-system) and $\delta_t \approx 14\%$ (G-system) (also shown by the plot of ϕ in Fig. 3). Above this δ the particles in the systems are dominated by fluid phase and hence no solid–liquid transition is possible, as indicated by the terminated values. Hence, the terminal polydispersities for U and G systems are 8% and 14%, respectively. This observation is in accordance with the earlier findings that beyond a terminal value of polydispersity (δ_t), crystallization, as well as the fluid-solid coexistence tends to vanish.[49–55] In addition, the terminal polydispersity is reported to occur anywhere between 5%–15%.[56] It is interesting to note that in the limit of small polydispersity ($\delta \leq 2\%$) the size-polydisperse system is insensitive to the type of distribution. In addition, the systems show no significant qualitative difference when polydispersity in mass is introduced. Despite the fact that mass polydispersity has an unappreciable impact on T^* in both systems, its function in the nature of ordering remains unknown and is discussed briefly in Section 4. We now move on to understand the role of polydispersity in the nature of particle ordering characterized by hexatic order parameter and pair correlation function.

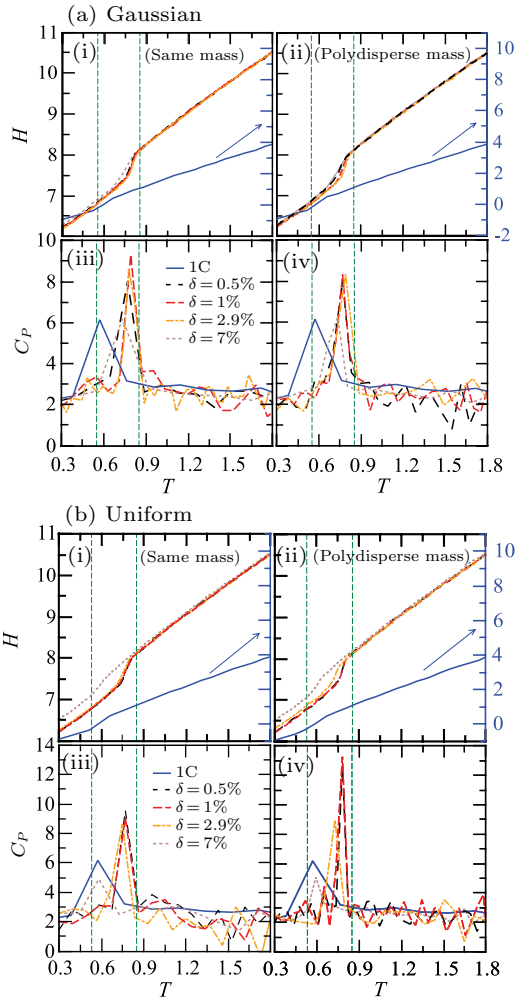


Fig. 2. Plot of enthalpy H (upper panel) and the corresponding heat capacity C_P (lower panel) for (a) Gaussian and (b) uniform systems at different values of δ indicated in the figure plotted together with 1C system (values indicated on the right). The region enclosed by the two vertical dash-lines marks the region where transition is observed.

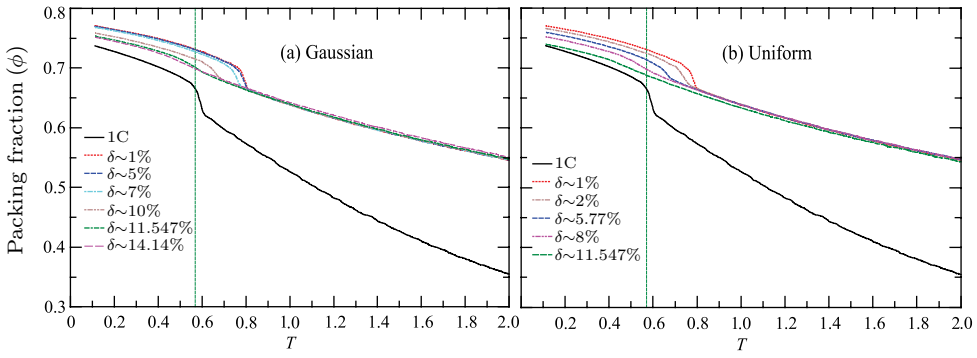


Fig. 3. Plot of packing fraction (ϕ) as a function of T for mass polydisperse systems. Packing efficiency greatly enhances with small introduction of δ in comparison to 1C system. (a) Gaussian distributed system, where the differences in the value of ϕ gradually diminish approaching its δ_t. (b) Uniform system, similar trend as that of G system is observed. Vertical dash line marks the transition point of 1C system, $T \approx 0.57$, where the sudden drop in the ϕ value is observed indicating the melting of solid to liquid.

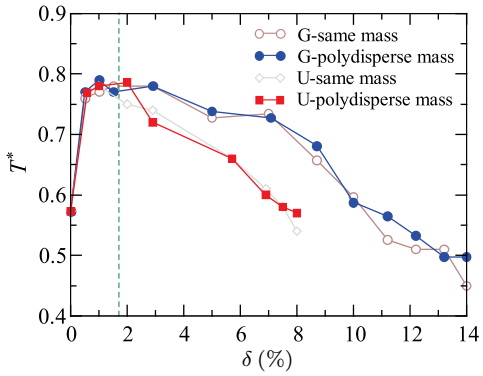


Fig. 4. Transition temperature (T^*) as a function of polydispersity (δ) for both the G and U systems. The vertical dash line is to guide the eyes indicating the limit beyond which T^* deviates. The higher values of T^* for G and U systems with small introduction of polydispersity are because of the increase in packing efficiency which enhances the ordering.

4. Spatial ordering and hexatic order parameter

The local orientation order of a particle located at r_j having M nearest neighbors is examined through the hexatic order parameter, $Q_6(r_j) = \frac{1}{M}\sum_{k=1}^{M} e^{i6\phi_{jk}}$, and ϕ_{jk} the angle between X-axis and the vector drawn from the center atom to the nearest neighbor particles.[12]

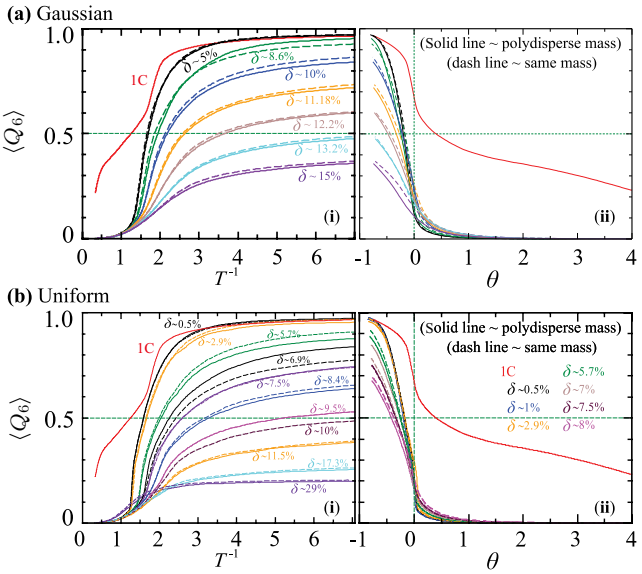


Fig. 5. Mean global hexatic parameter, $\langle Q_6 \rangle$ vs. T^{-1} at different values of δ indicated in the figure for (a)–(i) Gaussian and (b)–(i) uniform systems. The same plot as a function of reduced temperature, $\theta = (T - T^*)/T^*$, is shown on the right. The horizontal dash line indicates $\langle Q_6 \rangle = 50\%$ at $\theta = 0$. Note that with small δ, $\langle Q_6 \rangle$ approaches to that of 1C due to higher packing efficiency (see text for details).

In Fig. 5, the global hexatic order parameter $\langle Q_6 \rangle$ (i.e., averaged over all the particles) plotted as a function of inverse temperature is displayed for polydisperse systems, as well as the reference 1C system. For an ideal crystal/perfect hexagonal structure all particles must be trapped in a cage indicated by $Q_6 \geq 0.7$.[27] The strength of confinement/caging depends on T and δ as shown in the figure. The value of $\langle Q_6 \rangle$ grows as temperature decreases and saturates at a particular value, which depends on the value of δ. In general, the saturated (or low temperature) value of $\langle Q_6 \rangle$ decreases for increasing polydispersity and beyond a certain value of δ the value is less than 0.5, e.g., see curves corresponding to $\delta = 13.2\%$ (Gaussian) and $\delta = 10\%$ (uniform). The observed behavior is consistent with other studies where it is reported that increasing polydispersity at fixed volume fraction lowers the structural correlations, pressure, energy, and viscosity.[57] It is interesting to note that the decrease of $\langle Q_6 \rangle$ with increasing δ is relatively fast in the case of U systems, indicating a higher order hexatic ordering in the Gaussian system for a given value of δ. This may be understood from the fact that (for a given value of δ) the particle size spread from its mean value is wider in the uniform system and consequently there is a larger disparity which eventually diminishes the orientation correlation, as reflected by the smaller values of $\langle Q_6 \rangle$. It can be seen from Fig. 5 that the hexatic ordering approaches 1C values and is even significantly higher for small $\delta < 8\%$ and 3% (not shown) for G and U systems, respectively. This eventually suggests higher packing efficiency and ordering for small δ. Hence, the higher values of T^* for small polydispersities. Although it is well known that polydispersity acts against the formation of ordered structure but small δ, in contrast it enhances the packing efficiency leading to higher ordering, as shown in Fig. 3. In general, with δ, structural correlation decreases. However, at much larger δ, there is an increase in particle fractionation. Within the fractionated solid clusters, local orientational ordering is plausible, although $\langle Q_6 \rangle$ is small, as observed for $\delta = 29\%$ in the U system for wider temperature range. On the other hand, in addition to size, introduction of mass polydispersity slightly lowers $\langle Q_6 \rangle$ value in all the systems investigated. Finally, to highlight the difference in the growth of hexatic order around T^*, we plot $\langle Q_6 \rangle$ as a function of reduced temperature $\theta = (T - T^*)/T^*$ for both reference 1C system and size-polydisperse systems, see Fig. 5 (right-hand panel). In Fig. 6, the plot of $\langle Q_6 \rangle$ as a function of δ obtained at the respective T^* is displayed. For both G and U systems, $\langle Q_6 \rangle$ values are relatively high at small δ, even at the transition point that is well above the solid–liquid coexistence region. However, it decreases gradually with δ, as shown in Fig. 6. The effect of mass polydispersity on $\langle Q_6(T^*) \rangle$ for both the systems is insignificant in all polydispersity ranges.

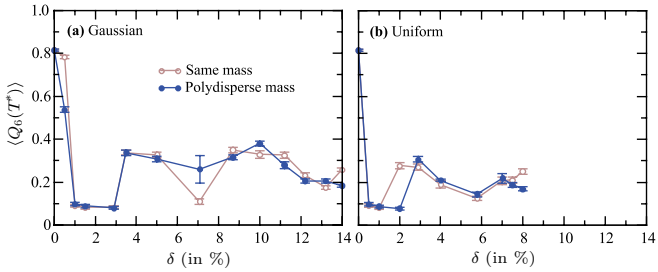


Fig. 6. Plot of average global hexatic parameter $\langle Q_6 \rangle$ at the transition (T^*) point for (a) Gaussian and (b) uniform distributed systems.

At a certain value of δ and T, the existence of solid and liquid phases is equally probable. This state is evidenced by $\langle Q_6 \rangle \approx 0.5$. At this particular value of T, both solid-like and liquid-like ordering are equally probable, i.e., $\langle Q_6 \rangle \approx 50\%$, and hence can be speculated as the coexistence of both solid and liquid phase.[27] Based on this, a phase diagram is constructed in the T–δ plane for the polydisperse system in the following manner. During a continuous cooling/heating cycle we monitor the growth/decay of $\langle Q_6 \rangle$ and note the temperature at which $\langle Q_6 \rangle = 0.5$ and thus in this manner a coexistence region or curve separating the solid-like ($\langle Q_6 \rangle > 0.5$) and liquid-like ($\langle Q_6 \rangle < 0.5$) regions are obtained, see Fig. 7. In order to quantify the presence of solid-like and liquid-like particles at the coexistence region, we examined the distribution of hexatic order parameter, Q_6, as shown in Fig. 8 for each δ at the coexistence temperature (indicated in Fig. 7). The distribution shows two peaks (above and below $Q_6 = 0.5$), which supports the coexistence of both solid and liquid-like particles for G as well as U systems. However, the 1C system exhibits a unimodal distribution with mean value of around 0.5. This suggests that the 1C system has a variety of hexagonal phases, ranging from isotropic liquid to solid-like, as seen by the distribution of Q_6 in the coexistence area. It is more likely for isotropic liquid (or hexagonally packed solid) to occur for temperatures slightly above (or below) T where $Q_6 \approx 50\%$.

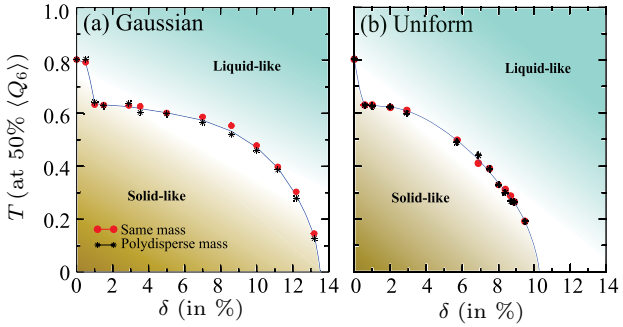


Fig. 7. Phase diagram in polydispersity index (δ) and temperature plane constructed from hexatic order parameter showing liquid-like ($\langle Q_6 \rangle < 0.5$) and solid-like ($\langle Q_6 \rangle > 0.5$) phases. Since at $\langle Q_6 \rangle \approx 0.5$, i.e., at approximately 50% hexatic ordering, the presence of solid-like and liquid-like particles is equally probable[27] (see text for detail). (a) G system and (b) U system. No significant difference between systems with the same mass particles and different masses is seen. The solid line is a guide to the data points indicated by solid circles and stars.

As one can see, the coexistence region extends to $\delta \approx 13.5\%$ for the Gaussian system and $\delta \approx 10\%$ for the uniform system (and vanishes beyond those values), and thus a larger coexistence region in the case of Gaussian system. In the case of uniform system the smaller particles (whose population is large compared to Gaussian system) get trapped in the interstitial sites of the bigger particles and eventually distort the hexatic ordering. An interesting difference is seen in the small δ limit, where for the uniform system the value of $\langle Q_6 \rangle$ drops to a smaller value for $0 < \delta < 0.5\%$, while for Gaussian system the drop to a similar value is seen for $\delta \geq 0.5\%$. Comparing both the systems, we see that for small increment in polydispersity, the T at which 50% $\langle Q_6 \rangle$ ordering is observed is much higher in magnitude in case of G system in contrast to the U system and approaches to that of the 1C system, which is well above their T^* value. Furthermore, increasing polydispersity sharply drops the $\langle Q_6 \rangle$ value due to decreasing ϕ, which then continues to decay until it vanishes on approaching 14% δ. To further comprehend the nature of particle ordering, we analyze the radial distribution of particle in the following section.

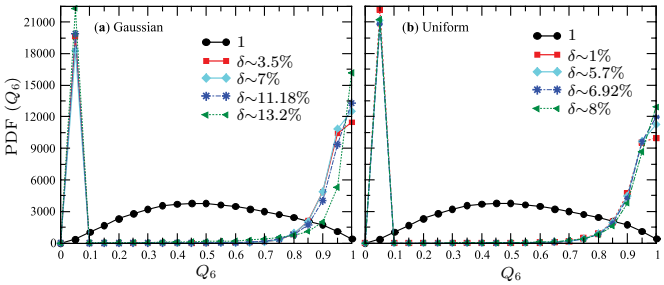


Fig. 8. The distribution of the hexagonal order parameter, Q_6, at the coexistence temperature indicated in Fig. 7 for different values of δ for both G and U systems (polydisperse mass). Sample over 10 equilibrated frames for each δ value. The presence of bimodal peaks suggests the presence of liquid-like ($Q_6 < 0.5$) as well as solid-like ($Q_6 > 0.5$) clusters for the polydisperse systems. See text for details.

Another means to comprehend the local ordering is by constructing Voronoi tessellation (VT), which depicts geometry of the system by dividing the space into regions based on the proximity to a set of points. However, in the physical systems (such as granular materials) particles are not simply points — they vary in shape and size. Traditional VT, which considers particles as points, may not adequately represent the geometry of polydisperse systems. To address this limitation, researchers have developed the concept of Set Voronoi tessellation (SVT), which considers a set of points on each particle's surface rather than individual points.[56] This technique gives a more realistic depiction of non-spherical or polydisperse particles spatial effect and enables the extraction of significant local information of systems composed of arbitrarily shaped particles. Figure 9 displays the SVT of uniform size distributed systems for $\delta = 10\%$ at three different T. The color bar on the left-hand (black-white) indicates particle diameter and that on the right-hand (blue-red) indicates the number of closest neighbors or coordination number (N_c). This figure clearly depicts how particle correlation fluctuates with temperature. At modest T values, the majority of particles have six close neighbors ($N_c = 6$), indicated by the hexagonal structure inducing stability in the system. With increasing T, the hexagonal shape is distorted and the particle correlation decays. This behavior is similar to the analysis of Q_6 and depends on the shape of the distribution. N_c varies with both T and δ. At small δ, most particles have $N_c = 6$ (not shown) and increases with δ due to the creation of smaller particles. This eventually destabilizes the system by distorting the ordering in the system.

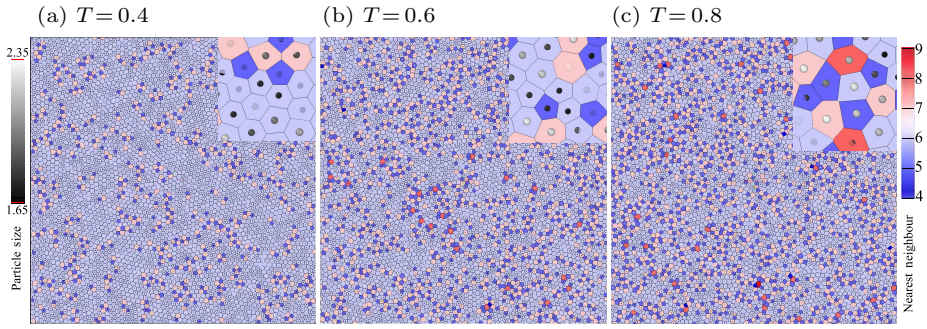


Fig. 9. Voronoi tessellation weighted by particle size for the uniform system ($\delta = 10\%$) at three different values of temperatures. The color bar from black to white (left-hand) shows particle diameter, while blue-white-red (right-hand) denotes particle nearest neighbor. Particle correlation shifts as temperature varies. The figure shows that for modest T values, the majority of particles have six closest neighbors. This behavior is similar for all δ values and distributions studied. Note that the particle size has been reduced for clarity.

5. Pair correlation

To look at the local ordering we calculate the radial distribution function, $g(r) = \frac{A}{N^2}\langle\sum_i\sum_{j\neq i}\delta(\boldsymbol{r}-\boldsymbol{r}_{ij})\rangle$, with $\boldsymbol{r}_{ij} = \boldsymbol{r}_i - \boldsymbol{r}_j$, $r = |\boldsymbol{r}|$, A and N are the area of the simulation box and number of particles, respectively.[45] In Fig. 10, we display pair correlation function obtained at three different values of reduced temperature $\theta = (T - T^*)/T^*$ around the transition for various δ. It is clear from figure that for small introduction of $\delta \approx 0.5\%$, the ordering is much enhanced in both the δ system and approach to that of the 1C below transition. The amplitude of oscillation of the first peak is consistently the highest in the δ system, indicating a higher order short range ordering which then decays gradually. It is expected that with increasing δ, the neighboring particles should increase. This is seen for $\delta > 2.9\%$ and 7% in Fig. 10. Note that the T^* for the δ systems are significantly higher than 1C, see Fig. 4. Hence, a small increment in T above transition significantly diminishes ordering, as is also observed in Fig. 3 where ϕ decay steeply with T approaching the transition region. This indicates that size-polydisperse systems (at the considered value of δ) lack long-range order, even at the transition point.

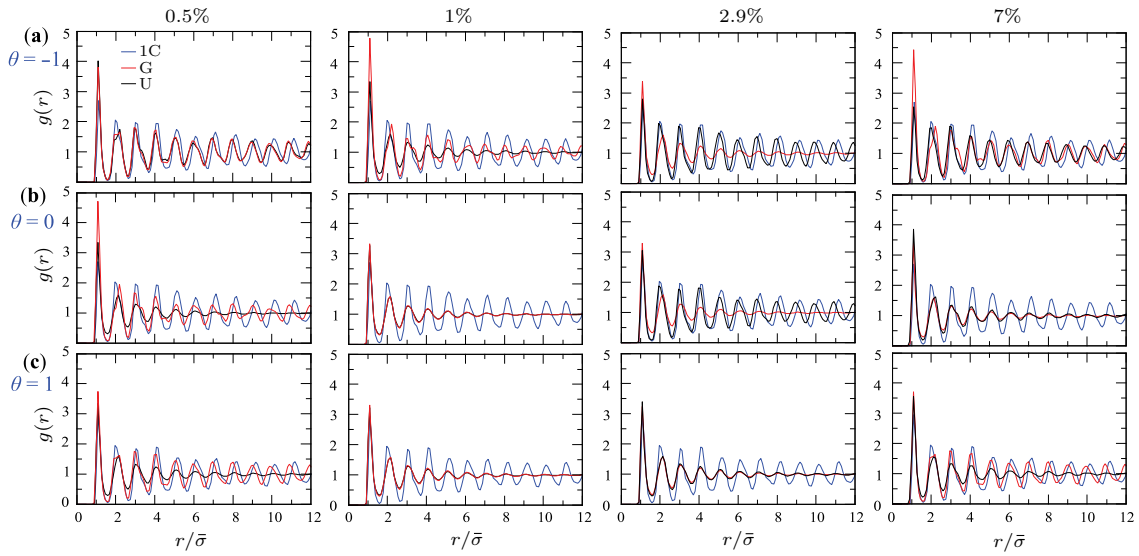


Fig. 10. Comparison of radial distribution function (rdf) or $g(r)$ for the G and U systems with the 1C system at and around T^* in reduced temperature θ, where $\theta = 0$ is the transition point, $\theta = -1$ and 1 represent the temperature 1% below and above the transition point, respectively, for three polydispersity indices. Around the transition point, the first order peak for δ systems is significantly higher than that of the 1C system due to enhanced positional correlation induced by packing efficiency and the higher order peaks rapidly decay with distance as compared to 1C. See SI for the case of polydisperse mass.

For all Ts under consideration, we find that the amplitude of oscillation is largest for 1C, followed by Gaussian and uniform size-polydisperse systems, respectively, and higher order peak positions are shifted to smaller values for polydisperse systems. The oscillation in both the G and U systems gradually decreases with increasing T, this happens because the presence of uncorrelated particles grows progressively with T, leading to structural decay, as indicated by the compressed transition ϕ value in Fig. 3. On further increasing δ, the presence of like and unlike particles becomes equally probable, where like particles group together forming distinct phases (see Fig. 1), eventually increasing the particles correlation.

It is evident from Fig. 10 that the curves below T^* closely follow each other for all temperatures but gradually decay above $\theta = 0$ with distance, as is evident from the shift of higher order peaks, which is an indication of the formation

of a liquid-like structure. This is akin for all polydisperse systems in the considered polydispersity ranges. The ordering of the particles is more perceptible with higher order peaks more pronounced in the lower θ in both the polydisperse systems as compared to the 1C system, owing to the fact that the presence of the smaller particles is more pronounced (see Fig. 1) in the polydisperse system because of higher packing efficiency. Since the particles' motion is dependent on the surrounding temperature, decreasing the temperature below T^* tends to lower the kinetic energy of the individual particles, the smaller particles get trapped in the six or higher order neighbors and eventually remain confined, leading to higher order neighbors with longer oscillation. These oscillations with higher order peaks gradually diminish with increasing temperature and eventually decay, a property of liquid-like structure. In the higher temperature regime, individual particles gain kinetic energy and can knock off the surrounding neighbors with ease creating defects. This knock-on effect continues distorting the shape of the structural order in the higher temperature regions for all systems. The ordering is more appreciable and pronounced, even above T^* in the 1C systems as compared to both the polydisperse systems for all θ values. A similar trend is observed for systems with polydisperse masses (see supplementary information). The nature of ordering can also be apprehended from the collective dynamics of the particle examined in the following section.

6. Dynamics

The particle dynamics are dependent on the local environment and we characterize the statistical nature of the particle dynamics through mean-square displacement (MSD), defined as

$$\langle \Delta r^2 \rangle = \frac{1}{N} \sum_{i=1}^{N} [\, \boldsymbol{r}_i(t) - \boldsymbol{r}_i(0)]^2, \tag{4}$$

where N is the number of particles, and $\boldsymbol{r}_i$ is the position of the i^{th} particle. To calculate MSD, we switch from NPT to NVT ensemble (to avoid artifacts due to volume fluctuation during NPT runs), where the temperature of the system is maintained using a Langevin thermostat. Since our main focus is on the effect of polydispersity on the dynamics, we confine our analysis for $T \to T^*$ (or $\theta \to 0$), where the differences in the dynamics between the systems are expected to magnify.

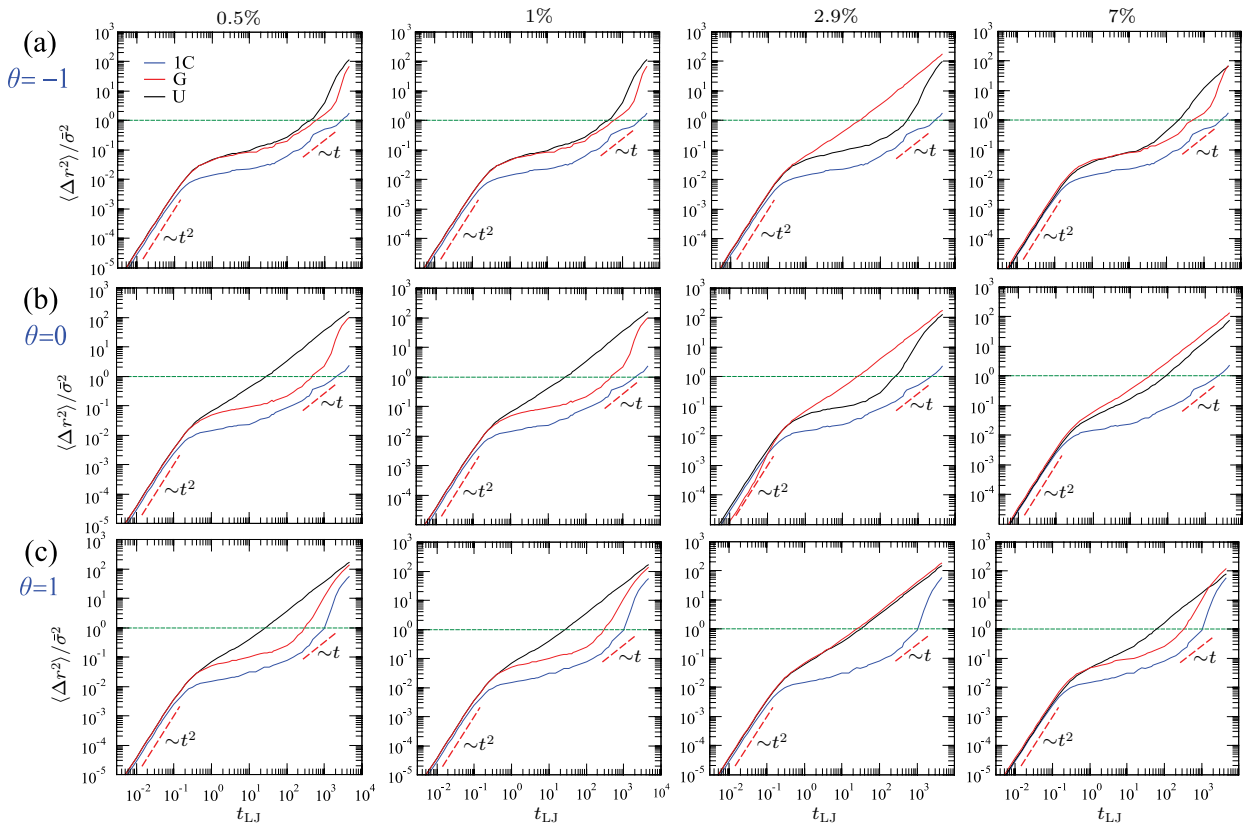


Fig. 11. MSD curves for Gaussian and uniform systems (same mass particles) at different values of δ (indicated at the top of the figure) together with reference 1C system. The curves are obtained at three different values of reduced temperature: (a) $\theta = -1$, (b) $\theta = 0$, and (c) $\theta = 1$ (in %). Horizontal dashed lines are drawn at $\langle \Delta r^2 \rangle / \overline{\sigma}^2 = 1$. See SI for the case of polydisperse mass.

The MSD curves obtained are shown in Fig. 11, where both inertial ($\Delta r^2 \sim t^2$, at short-times) and diffusive ($\Delta r^2 \sim t^1$, at long-times) regimes are observed for all the systems. Note that in some of the curves, e.g. Fig. 11(b), after reaching diffusive regime the MSD curves again go inertial/ballistic. This observed behavior may be related to the individual motion of the particles coupled with cooperative movement of the cluster (which the particle belongs to) at this time scale. However, at

sufficiently long time, the curve again crosses over to diffusive behavior. An interesting quantity of relevance is the mean relaxation time, τ, defined as the average of the time taken by the particles to cover their own sizes. From the MSD curves τ values are extracted by looking at the time where $\langle \Delta r^2 \rangle / \overline{\sigma}^2 = 1$. In general, with a decrease in temperature the relaxation time increases for all systems because with lowering T it becomes harder for a particle to escape the cage formed by its neighboring particles, see the value of time where $\langle \Delta r^2 \rangle / \overline{\sigma}^2 = 1$ shifting to higher value with lowering θ for a given δ in the figure. Furthermore, it is clear from the figure that τ for the size-polydisperse systems is small compared to the 1C system. This suggests a higher caging effect as well as ordering in monodisperse system, as expected. For $T < T^*$, a strong caging effect (indicated by the relatively broad plateau at intermediate times) is observed in all the systems. An interesting observation, at the transition temperature ($\theta \approx 0$) is that for $\delta \leq 1\%$ the relaxation time for U-system is $\tau_U \approx 30\tau_{LJ}$, while for G-system it is $\tau_G \approx 500\tau_{LJ}$, which is an order of magnitude larger and the value is closer to the 1C system. When increasing polydispersity further, i.e., $\delta \geq 2.9\%$ in the figure, the caging effect is more pronounced in the uniform distributed systems at and below the transition, but for $\theta > 0$ (or $T > T^*$) both the systems shows comparable MSD curve. This behavior may be understood from the fact that at a given δ the particles spreading from the mean are consistently the highest in the uniform systems and consequently smaller particles get trapped in the interstitial sites of the bigger particles, enhancing the caging effects by the formation of higher order neighbors, although distorting the hexatic phase. Overall, with the increase of δ, the caging effects gradually increase in both the polydisperse systems. In Fig. 12, we display the mean relaxation time as a function of polydispersity index for both Gaussian and uniform systems (and same mass and polydisperse mass cases). The observed trend is that τ decreases with increasing δ (although some non-monotonicity for $\theta \leq 0$), and hence an increase of diffusion constant is expected for higher polydisperse systems, which is consistent with other works.[59] The effect of mass polydispersity on the dynamics is reflected in the relaxation dynamics for both systems around the transition, where it is observed that the value of τ is consistently higher (than the same mass case) and thus there is a slower structural relaxation.

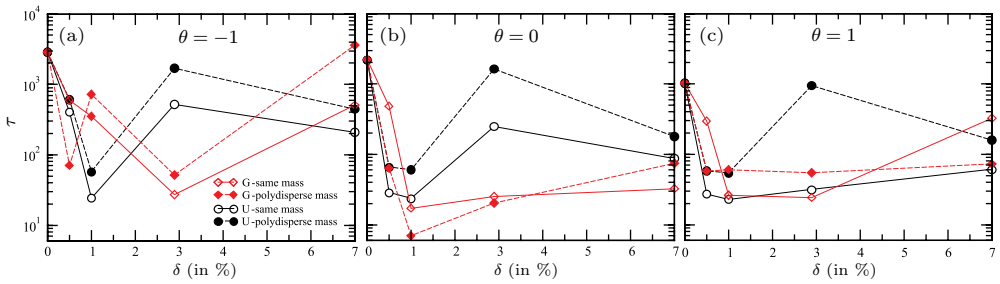


Fig. 12. Relaxation time (τ) as a function of polydispersity for different values of reduced temperature (θ). Filled symbols represent the data points for polydisperse mass and the open symbols are for the same mass for both the Gaussian (G) and uniform (U) systems, respectively.

7. Conclusion

In this work we provide an in-depth analysis of the effect of size and mass polydispersity on the melting/freezing transition and its consequence on the solid–liquid phase diagram, and statics and dynamics in general of a model LJ fluid in 2D. It is observed that, irrespective of the types of size distribution considered, the introduction of size-polydispersity leads to elevation of T^* (w.r.t. monodisperse system) due to an increase in the packing fraction, which then decreases upon a further increase of δ and terminates at $\delta \approx 8\%$ (U-system) and $\delta \approx 14\%$ (G-system), where the transition gets broadened and diminishes. Increasing polydispersity also decreases the particle correlations, thereby decreasing the global hexatic order parameter, $\langle Q_6 \rangle$. The $\langle Q_6 \rangle$ values for U systems are consistently the lowest in comparison with G systems for the same value of δ. The phase diagram in T–δ plane indicates that the solid–liquid coexistence is wider for the G-systems due to the relatively narrow particle size distribution as compared to the U-system. Furthermore, the analysis of $\langle Q_6 \rangle$ indicates that the local particle ordering is higher in the smaller polydispersity ranges and ordering increases with lowering temperature, as is also shown by the qualitative analysis of the pair correlation function. The effect of mass polydispersity on the particle ordering manifested from the dynamics of the individual particle motion is consistently the highest for 1C in comparison with the polydisperse systems in all temperature ranges, consequently suggesting a higher structural order.

It is important to point out that here we have investigated only the Gaussian and uniform particle-size distributions. However, other distributions such as log-normal distribution and Weibull distribution are also important because they represent many naturally occurring size distributions. For instance, log-normal distribution is often used to describe particle size distributions in materials science, and the Weibull distribution is commonly applied in reliability engineering and failure analysis. On the other hand, studies related to transport properties of size-polydisperse fluids have not been ex-

plored enough to date for lower dimensional systems. Hence, we shall explore the behavior of transport properties such as thermal conductivity and viscosity considering a wide variety of size-distribution functions in our upcoming work.

Data availability statement

The data that support the findings of this study are available from the corresponding author upon reasonable request.

Acknowledgement

JP acknowledges NFST fellowship (Award No. 201920-NFST-NAG-02957).

References

[1] Adachi Y, Fijihara I, Takamiya M and Nakanishi K 1988 *Fluid Phase Equilibria* **39** 1
[2] Galliéro G, Boned C and Baylaucq A 2005 *Ind. Amp. Eng. Chem. Res.* **44** 6963
[3] Galliéro G, Boned C and Fernández J 2011 *J. Chem. Phys.* **134** 064505
[4] Bohn M, Lustig R and Fischer J 1986 *Fluid Ph. Equilibr.* **25** 251
[5] Barker J A, Henderson D and Abraham F F 1981 *Physica A* **106** 226
[6] Nasrabad A E, Laghaei R and Deiters U K 2004 *J. Chem. Phys.* **121** 6423
[7] Fasolo M and Sollich P 2003 *Phys. Rev. Lett.* **91** 068301
[8] Pagonabarraga I, Cates M E and Ackland G J 2000 *Phys. Rev. Lett.* **84** 911
[9] Kosterlitz J M and Thouless D J 1973 *J. Phys. C: Solid State Phys.* **6** 1181
[10] Kosterlitz J M and Thouless D J 1972 *J. Phys. C: Solid State Phys.* **5** L124
[11] Nelson D R and Halperin B I 1979 *Phys. Rev. B* **19** 2457
[12] Halperin B I and Nelson D R 1978 *Phys. Rev. Lett.* **41** 121
[13] Frenkel D and McTague J P 1979 *Phys. Rev. Lett.* **42** 1632
[14] Wierschem K and Manousakis E 2011 *Phys. Rev. B* **83** 214108
[15] Evans R M L 1999 *Phys. Rev. E* **59** 3192
[16] Ingebrigtsen T S and Tanaka H 2016 *J. Phys. Chem. B* **120** 7704
[17] Ingebrigtsen T S and Tanaka H 2015 *J. Phys. Chem. B* **119** 11052
[18] Wilding N B, Sollich P, Fasolo M and Buzzacchi M 2006 *J. Chem. Phys.* **125** 014908
[19] Shagolsem L S, Osmanović D, Peleg O and Rabin Y 2015 *J. Chem. Phys.* **142** 051104
[20] Shagolsem L S and Rabin Y 2016 *J. Chem. Phys.* **144** 194504
[21] Eastwood A R 1981 *J. Chem. Soc., Faraday Trans.* **77** 1411
[22] Murarka R K and Bagchi B 2003 *Phys. Rev. E* **67** 051504
[23] Gotze W and Sjogren L 1992 *Rep. Prog. Phys.* **55** 241
[24] Bengtzelius U, Gotze W and Sjolander A 1984 *J. Phys. C: Solid State Phys.* **17** 5915
[25] Ingebrigtsen T S and Dyre J C 2023 *J. Phys. Chem. B* **127** 2837
[26] Patashinski A Z, Ratner M A, Grzybowski B A, Orlik R and Mitus A C 2012 *J. Phys. Chem. Lett.* **3** 2431
[27] Patashinski A Z, Orlik R, Mitus A C, Grzybowski B A and Ratner M A 2010 *J. Phys. Chem. C* **114** 20749
[28] Salacuse J J and Stell G 1982 *J. Chem. Phys.* **77** 3714
[29] Sollich P and Cates M E 1998 *Phys. Rev. Lett.* **80** 1365
[30] Warren P B 1998 *Phys. Rev. Lett.* **80** 1369
[31] Reichhardt C O and Reichhardt C 2003 *J. Phys. A: Math. Gen.* **36** 5841
[32] Reichhardt C and Reichhardt C O 2005 *Phys. Rev. E* **71** 062403
[33] Chen J X, Yuan R, Cui R and Qiao L 2021 *Nanoscale* **13** 1055
[34] Ruiz P S, Lei Q L and Ni R 2019 *Commun. Phys.* **2** 70
[35] Pal, Sayan, *et al*. 2023 *Chemical Engineering Journal* **462** 142007
[36] Horta-Pineres, S, *et al*. 2020 *Appl. Phys. A* **126** 1
[37] Phongtongpasuk, Siriporn, Sarinya Poadang and Niti Yongvanich 2016 *Energy Procedia* **89** 239
[38] Singh, Priyanka, *et al*. 2016 *Artificial cells, nanomedicine and biotechnology* **44** 1569
[39] Pigolotti S, López C, Hernández-García E and Andersen K H 2010 *Theoretical Ecology* **3** 89
[40] Lai C D, Murthy D N and Xie M 2006 *Springer Handbooks* pp. 63–78 (Springer)
[41] Matsumura Y and Jackson T L 2014 *Phys. Fluids* **26** 123302
[42] Wilding N B and Sollich P 2010 *J. Chem. Phys.* **133** 224102
[43] Sarkar S, Biswas R, Santra M and Bagchi B 2013 *Phys. Rev. E* **88** 022104
[44] Pame J and Shagolsem L S 2021 *Macromol. Symp.* **399** 2100037
[45] Allen M P and Tildesley D J 2017 *Computer simulation of liquids*, Oxford University Press
[46] Frenkel D and Smit B 2001 *Understanding Molecular Simulation: From Algorithms to Applications* (Cambridge: Academic Press)
[47] Plimpton S 1995 *J. Comput. Phys.* **117** 1
[48] Urikhinbam S S and Shagolsem L S 2023 *J. Phys. Chem. B* **127** 2739
[49] Pusey P N 1987 *J. Phys.* **48** 709
[50] Barrat J L and Hansen J P 1986 *J. Phys.* **47** 1547
[51] McRae R and Haymet A D J 1988 *J. Chem. Phys.* **88** 1114
[52] Dickinson E, Parker R and Lal M 1981 *Chem. Phys. Lett* **79** 578
[53] Dickinson E and Parker R 1985 *J. Physique, Lett.* **46** 229
[54] Bolhuis P G and Kofke D A 1996 *Phys. Rev. E* **54** 634
[55] Dullens R P and Kegel W K 2004 *Phys. Rev. Lett.* **92** 195702
[56] Kofke D A and Bolhuis P G 1999 *Phys. Rev. E* **59** 618
[57] Abraham S E, Bhattacharrya S M and Bagchi B 2008 *Phys. Rev. Lett.* **100** 167801
[58] Volkel S and Huang K 2020 *In Traffic and Granular Flow*, 2019 pp. 429–437, Springer International Publishing
[59] Meitei T P and Shagolsem L S 2024 *Pramana* **98** 1